Classification of 3D UAS-SfM Point Clouds in the Urban Environment

Simiso Ntuli[1], Angus Forbes[2]

[1]Department of Land Surveying, School of Agriculture, Engineering and Science, University of KwaZulu-Natal, Durban, South Africa, 215017855@stu.ukzn.ac.za
[2]Department of Land Surveying, School of Agriculture, Engineering and Science, University of KwaZulu-Natal, Durban, South Africa

DOI: http://dx.doi.org/10.4314/sajg.v12i.2.6

Abstract

The classification of three-dimensional (3D) point clouds derived through the use of cost-effective and time-efficient photogrammetric technologies can provide helpful information for applications, particularly in the mapping context. This paper presents a practical study of 3D Unmanned Aerial System (UAS) – Structure-from-Motion (SfM) point cloud classification using mainly open-source software. Following a supervised classification approach that makes use of only the dimensionality of points, the entire scene was classified into three land-cover categories: ground, high vegetation, and buildings. By applying the above-mentioned approach, the level of competence in classifying a 3D point cloud of a heterogeneous scene situated in the University of KwaZulu-Natal, South Africa, was evaluated. The resulting overall classification accuracy of 81.3%, with a Kappa coefficient of 0.70, was determined by means of a confusion matrix. The results achieved indicate the potential use of open-source software and 3D UAS-SfM point cloud classification in mapping and monitoring complex environments and in other applications that might arise.

Keywords: *Classification, 3D Point Cloud, Unmanned Aerial Systems, Structure-from-Motion*

1. Introduction

Unmanned Aerial System (UAS)-based photogrammetry has proven to be a cost-effective method of acquiring point cloud data (Liu and Boehm, 2015). A point cloud is a collection of points, each associated with XYZ coordinates in a three-dimensional (3D) coordinate system. Additional information, such as reflectivity values and colour, may be included in a point cloud (Van Genechten, 2008). The ability of UASs to perform a simultaneous collection of high-resolution imagery and to generate a photogrammetric point cloud poses a unique advantage, thus allowing for a wide range of applications (Gevaert et al., 2016). Classified point cloud data are useful in a wide range of applications, including but not limited to environmental modelling, navigation and cultural heritage (Grilli et al., 2017; Roynard et al., 2018; Croce et al., 2021). Other disciplines, such as forestry, geomorphology, agriculture and damage assessment, have relied on point cloud classification for solutions (Wallace et al., 2012; Zhang and Kovacs, 2012; Gevaert et al., 2016).

Classifying LIDAR data into different land-cover categories has been at the centre of attention in many studies (Sithole and Vosselman, 2004; Antonarakis et al., 2008). Moreover, high financial costs are involved in acquiring LIDAR point clouds. However, using new technologies to generate 3D UAS Structure-from-Motion (SfM) point clouds is time-efficient and cost-effective. Numerous studies have focused on classifying natural environments into primary classes (Vandapel et al., 2004; Lalonde et al., 2006; Brodu and Lague, 2012; Jurado et al., 2020). The present study focuses on classifying point clouds in heterogeneous urban environments.

The initialism SfM originated from the computer vision community which denotes that the structure is created from images captured by a moving sensor (Westoby et al., 2012). SfM photogrammetric techniques can produce high-quality point clouds at a low cost. Firstly, a sparse point cloud is produced in bundle adjustments (Snavely et al., 2008). Subsequently, Clustering for Multi-View Stereo (CMVS) and Patch-based Multi-view Stereo (PMVS) algorithms are implemented to derive a densified point cloud (Furukawa and Pounce, 2009; Furukawa et al., 2010).

Point cloud classification is the operation of classifying and assigning some semantics to a group of points (Weinmann et al., 2015). Supervised, unsupervised, and interactive classification approaches are commonly used to assign class labels (Grilli et al., 2017). The automatic classification of point cloud information is essential and challenging at the same time. State-of-the-art includes both shallow and deep-learning techniques (Roynard et al., 2018). Researchers have applied different classification algorithms; Becker et al. (2018), for instance, used geometry and colour information to classify photogrammetric point clouds. Furthermore, in addition to the geometry, and owing to the incorporation of colour information, improved classification results were subsequently obtained. Conditional Random Fields (CRF), used by Niemeyer et al. (2012) to classify 3D urban scenes, have produced results with a high potential in classifying urban scenes. The CRF technique is based on a non-linear decision surface that accurately isolates the object groups in feature space. Brodu and Lague (2012) developed a semi-supervised classification algorithm that uses the dimensionality of points at multiple scales to classify LIDAR point clouds. Numerous researchers have used this classification algorithm: Grilli et al. (2017), for instance, analysed popular algorithms and techniques for 3D point cloud classification. Stones and vegetation in their archaeological site were filtered successfully. Farella (2016) automatically separated artificial and natural structures for mapping 3D underground environments. Another study conducted by Bonneau and Hutchinson (2019) identified and interpreted the geomorphological processes occurring along a cliff face by separating vegetation and granular material.

This study aimed to evaluate the use of 3D UAS-SfM point clouds to classify heterogeneous urban environments for mapping and monitoring, and for other applications that might arise. Furthermore, it aimed to assess the accuracy of the classified 3D UAS-SfM point cloud. As such, it was successful in using a multi-scale dimensionality criterion, to classify a modern heterogeneous environment into three land-cover categories, namely, ground, buildings and high vegetation. Based on training on small samples, classifiers that could be applied to unknown scenes were developed.

2. Study Area

The University of KwaZulu-Natal (UKZN), Howard College Campus, was selected for this study. It is situated in the environmental conservancy area of Glenwood, Durban (UKZN, 2017). The Howard College Campus sports field comprises various land-cover categories, including but not limited to grass, tarred and concrete surfaces, buildings and trees. Figure 1 shows an orthophotograph of the UKZN Howard College sports field.

Figure 1: Orthophotograph of the UKZN Howard College Campus sports field.

3. Materials and Methods

3.1. Materials

The apparatus used included a DJI Phantom 3 Professional UAS as the primary instrument for this study and a Trimble R4 GNSS receiver. The UAS was used to capture the images of the study area. It is equipped with a CCD camera with a resolution of 12 megapixels and an image size of 4000 by 3000. Additionally, the aircraft is remote-controlled and has satellite positioning systems (GPS/GLONASS) to allow for the navigation and geotagging of aerial images (DJI, 2017). The Trimble R4 model 3 GNSS receiver was used to measure the ground control points (GCPs). This instrument provides high accuracies for static GNSS, post-processed, and real-time kinematic surveying styles (GEOIM, n.d.). Moreover, various software programmes were used, including PrecisionFlight for creating and controlling the UAS flight mission and Web Open Drone Map (WebODM) to process the UAS images. Python 2.7, Pip, Windows Powershell and Docker were used to run WebODM. MATLAB R2018b programming language was used for camera calibration. To georeference the orthophotographs, Arc Map 10.7.1 was used. Lastly, the Pix4D Mapper trial version and CloudCompare 2.11 Alpha performed the point cloud classification.

3.2. Methods

The methods employed in this study are discussed in this section. The phases involved are as follows: (i) UAS camera calibration, (ii) acquisition of UAS Imagery, (iii) GNSS survey, (iv) 3D point cloud generation, (v) point cloud classification and (vi) accuracy assessment of point cloud classification.

3.2.1. UAS Camera Calibration

In computer vision and photogrammetric applications, camera calibration is a fundamental tool to determine the intrinsic and extrinsic camera parameters and to allow for the use of a camera as a measuring device (Nedevschi *et al*., 2002; Fetić *et al*., 2012). Moreover, in UAS mapping, low-cost digital cameras mounted as payloads are often used. Hence, camera calibration is considered to be crucial in obtaining mapping measurements of high accuracy (Yusoff *et al*., 2017). Tiscareño *et al*. (2019) studied different camera calibration methods on a camera-projected measuring system. Among these was a Zhang calibration method which accounts for and compensates for decentring, radial and prism distortions. This study concluded that compared to the Tsai and Direct Linear Calibration methods, the Zhang method provides better results in that it reveals only minor errors in the measurement results and extrinsic parameters. Therefore, the camera calibration toolbox based on the algorithm by Zhang (2000) was adopted for this study.

3.2.2. UAS imagery

Before any aerial photogrammetric project, flight planning is necessary to ensure reliability, precision and effectiveness in the acquisition of images (Hernandez-Lopez *et al.*, 2013). A visual inspection of the research area was conducted to find information about the site and to determine the land-cover categories to be classified in the 3D point cloud. A grid flight plan was created using the Precision Flight application, with the flight mission parameters listed in Table 1.

Table 1: Flight mission parameters

Parameter	Measurement
Area	4.9 hectares
Flying height	60m
Mission Duration	7min 53 sec
Overlap	80%
Sidelap	70%
Resolution	2.6cm/px

The UAS flight missions might be affected by weather conditions, specifically the wind (Wheeler *et al*., 2006). In fact, the presence of strong wind consumes more battery from the UAS as it tends to counteract the movement caused by the wind. This is important in this context as it is crucial that the drone should be stable in the air (Calvo *et al*., 2017). Therefore, the data were collected on a clear day with favourable atmospheric conditions. During this mission, a DJI Phantom 3 professional UAS

equipped with a digital CCD camera as a payload was used to capture 90 vertical images in auto-flight mode.

3.2.3. GNSS survey

To achieve the best in accuracy, the GCPs should be placed around the edges of the study area. However, by applying a stratified distribution and by arranging the GCPs within the project area, it is also possible to improve the vertical accuracy (Martínez-Carricondo *et al*., 2018). Henrico *et al*. (2016) evaluated the geolocation accuracy of high-resolution satellite ortho-images by using different ground control methods. The findings from their research indicate that manual GCPs produce a more accurate ortho-image in terms of positional accuracy. The GCPs in the current study were measured by using a method that was similar to the one applied throughout the fieldwork in the study by Henrico *et al*. (2016). A connection to a virtual reference station (VRS) was established and site calibration was performed with reference to the published South African trigonometrical beacons. The GCPs and check points were measured on-site by using the Trimble R4-3 GNSS receiver. These points were positioned around the edges and evenly distributed within the study area. All points were surveyed as observed control points to increase the accuracy of the measurements. Furthermore, the measured coordinates of the GCPs were used to georeference the orthomosaic and the 3D point cloud.

3.2.4. 3D point cloud

For this research study, WebOpenDroneMap (WebODM) was used to generate a 3D point cloud and other photogrammetric products with a ground sampling distance (GSD) of 0.025m. WebODM is a free and open-source API (Application Programme Interface) to the OpenDroneMap (ODM) software and requires that Python, Pip and Docker be integrated to run the WebODM programme. The afore-mentioned can be achieved by making use of the Git or Windows Powershell command line (WebODM, 2021). Even though a 3D point cloud and other photogrammetric products were generated using WebODM, Pix4D Mapper was also used to generate the same products. This was performed to facilitate comparative studies of the point clouds that were produced. Pix4D Mapper is a photogrammetric software programme for processing drone images (Pix4DSA, 2019). Unlike WebODM, Pix4D Mapper does not require any programming skills. Both programmes use the SfM technique to derive photogrammetric products. However, for this research, WebODM was the specific programme that produced a 3D point cloud of high density.

3.2.5. Point cloud classification

The main classification was performed using the CloudCompare software. However, Pix4D Mapper was also used to compare the classification results of both algorithms. The classification tool incorporated into Pix4D Mapper uses pixel values and geometry to classify points. This classification algorithm is completely unsupervised. Hence, the operator has no control over the training of classifiers. However, the tools for managing and refining the classification are provided (Pix4D, 2021). Pix4D Mapper comprises pre-established classification categories. The automatic classification was performed to filter the ground, high vegetation and buildings classes.

The supervised classification was performed using the *CAractérisation de NUages de POints* (CANUPO) plugin incorporated into CloudCompare. CANUPO is based on the local dimensionality characteristics of points in a point cloud. Points can be classified as 1D, 2D, or 3D, depending on a specified scale and location. For example, consider a site consisting of a power line, a ground surface, trees, and buildings. At a scale of a few centimetres, the ground surface and the building walls will appear as 2D and the trees as a mixture of 1D (branches) and 2D (leaves). At a sizeable scale (~50cm), the ground surface will still come across as 2D, and the trees will appear in 3D, while the power lines will remain as 1D (Brodu and Lague, 2012).

The combination of information from various scales results in signatures that recognise several classes of objects in the scene. These signatures are automatically generated through the training point, thus enabling optimization of class separability. A combination of information from various scales contributes toward the creation of descriptors that are able to recognize other object classes present in the scene. The creation of a classifier involves two steps: firstly, the data are projected onto a plane of maximal separability; secondly, the classes in that plane are separated through a boundary. CANUPO is a binary classifier; therefore, when the classifier is applied, a point cloud is divided into two subsets, and only one classifier is permitted at a time (Brodu and Lague, 2012). Once a classifier has been created, a classification confidence value is provided. In that it uses the number of points present in each class, Equation 1 (Brodu and Lague, 2012) is used to determine the balanced accuracy measure that indicates the classifier performance. On the other hand, Equations 2 and 3 (Brodu and Lague, 2012) are used to determine the accuracy of the two classes.

$$ba = \frac{1}{2}\left(a_v + a_g\right) \quad [1]$$

$$a_v = \frac{t_v}{t_v + f_g} \quad [2]$$

$$a_g = \frac{t_g}{t_g + f_v} \quad [3]$$

Where:

ba - Balanced accuracy

v - Particular class v

g - Particular class g

a_v - Accuracy of v

a_g - Accuracy of g

t_v - Number of points truly classified as v

t_g - Number of points truly classified as g

f_v - Number of points falsely classified as v

f_g - Number of points falsely classified as g

The Fisher Discriminant Ratio (*fdr*) is used to evaluate the separability of the classes. A large value of *ba* denotes a good recognition measure. Likewise, well-separated classes are denoted by a high value for the *fdr* (Brodu and Lague, 2012). Equation 4, derived from Brodu and Lague (2012) and Theodoridis and Koutroumbas (2008), was used to determine the *fdr*, where μ_c and v_c represent the average and variance of d for class c; d is a signed distance to the separation line.

$$fdr = \frac{(\mu_2 - \mu_1)^2}{(v_1 - v_2)} \quad [4]$$

The training data were extracted from the point clouds in different areas. The former were also generated by applying the SfM technique. Training samples were merged to increase the chances of creating classifiers with a high recognition rate. Two classifiers were created; Classifier A was trained to filter ground from non-ground points, while Classifier B filtered high vegetation and buildings from the remaining points. Both classifiers were trained at 12 different scales. The scales ranged from as small as 0.04m to 50m and were selected on account of their improved separability rate. Since CANUPO is a binary classifier, the filtering of multiple classes is a complicated process in that it, allows only two classes at a time. A hierarchical classification procedure, as shown in Figure 2, was used to classify the entire point cloud.

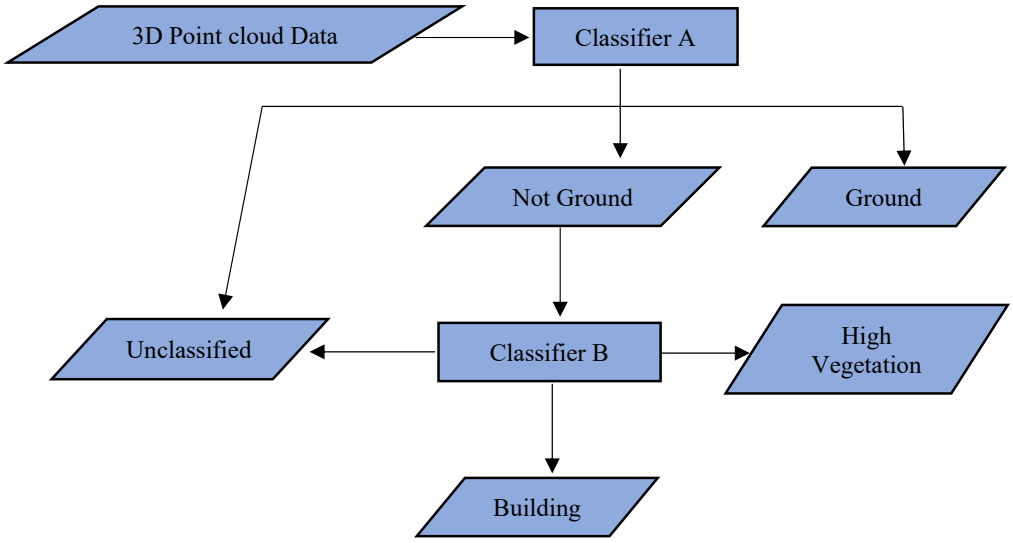

Figure 2: Proposed hierarchical classification procedure.

3.2.6. Accuracy assessment

Point cloud classification accuracy was evaluated using a georeferenced orthophoto generated from aerial imagery. Ground truth sites were randomly selected from the orthophoto to validate the classification. The point clouds were georeferenced before classification in Pix4D Mapper and CloudCompare. The ArcMap programme was used to facilitate the validation of the classified points against the ground truth site. A site visit was also conducted.

The qualitative assessment approach applied by Sithole and Vosselman (2004) for classifying bare earth and object classes was used to assess the competence of the classification. This approach is based on visual inspection and comparison of the classified points. Associated errors of omission (EO) and commission (EC) (Type I and Type II errors) were identified. The performance of filtering algorithms provided by both Pix4D Mapper and CloudCompare was evaluated. The CANUPO classification results were further assessed quantitatively by using a confusion matrix to determine the accuracy and the kappa coefficient to determine reliability. Random check points were generated over the entire extent of the study area by using Arc Map. This was performed to eliminate bias in the selection of the check points. However, because no points were randomly allocated, a few points were manually added to the buildings category.

4. Results and Analysis

4.1. UAS camera calibration

The intrinsic parameters of the camera lens resulted in a focal length of 3.64mm +/- 0.10mm, which is almost 3.61mm per the specifications of the camera. The value of the pixel error was found to be [0.28 0.21] pixels, which is very small. The overall calibration process indicates an excellent state of the camera for use as a measuring device. Table 2 shows the calibration results with uncertainties.

Table 2: Camera calibration results

Parameter	Value
Focal length (fc)	[2346.62700 2349.88146] +/- [61.58243 61.28156] microns
Principal point (cc)	[2014.79146 1510.17880] +/- [5.93212 9.38874] mm
Skew (alpha c)	[0.00000] +/- [0.00000]
Angle of pixel axes	90.00000 +/- 0.00000 degrees
Distortion (kc)	[-0.00318 -0.00460 0.00293 -0.00042 0.00000] +/- [0.00348 0.00613 0.00057 0.00048 0.00000]
Pixel error	[0.28358 0.20695] pixels

4.2. Georeferencing

Georeferencing is the transformation from a local to a global coordinate system. It requires a minimum of three common and identifiable targets in both coordinate systems (Van Genechten, 2008). In this study, the GCPs were used as the targets for georeferencing. They are necessary when conducting aerial surveys since they bring the projected to the spatial coordinate system and improve the accuracy of the data obtained (Garcia and Oliveira, 2020; Geavis, 2020). Moreover, they make it possible for real-world measurements to be obtained from the georeferenced spatial data. Boon *et al*. (2016) investigated the use of UAS photogrammetry as a tool to map wetlands. This study assessed the geometric accuracy, obtaining 0.018m and 0.0025m for the overall and vertical Root Mean Square Errors (RMSEs). The results obtained indicate that UAS photogrammetry can produce photogrammetric products of high accuracy for application to the mapping of wetlands. In the current

study, the point cloud georeferencing performed using 3D GCPs in Pix4D Mapper and CloudCompare indicated good results at an average GSD of 0.025m. In this case, overall RMSEs of 0.032m and 0.053m were achieved, respectively. According to these results, the accuracy obtained is comparable to that of a study by Lucieer *et al.* (2014), where UAS-SfM photogrammetry was employed and an overall RMSE of 0.042m was obtained, thus beating the RMSE of 0.09m by Ouédraogo *et al*. (2014).

4.3. Point cloud classification

Points were classified into appropriate land-cover categories. However, misclassifications were noticed in each category. The classification results obtained using Pix4D Mapper show the category of interest while other categories were subtracted/hidden from the classified point cloud. For example, to show the high vegetation category, all other points were removed, isolating only this category. Figure 3 below shows the classification results obtained using Pix4D Mapper.

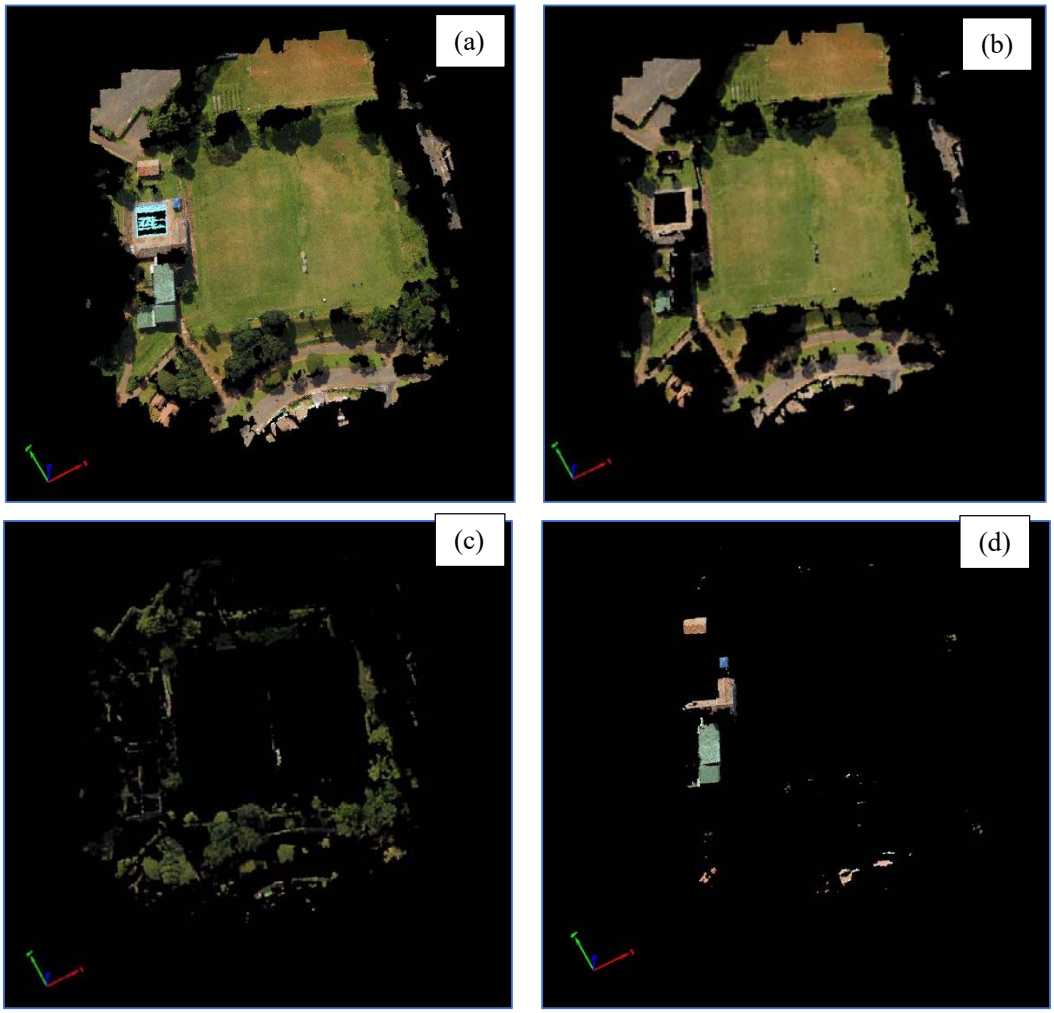

Figure 3: (a) Study area before classification; (b) Classified point cloud showing ground; (c) Classified point cloud showing high vegetation; and (d) Classified point cloud showing buildings.

In every classified land-cover category, errors of commission and omission were present. The Type I error was dominant across all classes, except for the ground category, which was mainly affected by the Type II error. Visual inspection of the overall classification indicated satisfactory results. Misclassifications were addressed by manually allocating points to the appropriate land-cover categories.

The CANUPO classification conducted using CloudCompare provided excellent results during the classifier training phase. Classifier A achieved a ba value of 0.994 and an fdr value of 6.826. On the other hand, a ba value of 0.957 and an fdr value of 6.038 were achieved for Classifier B. Classification thresholds of 90% and 85% were used for Classifier A and B, respectively, resulting in the correct classification of more points. Figure 4 shows the CANUPO classification results. The statistics of classified points are shown as a percentage in Figure 5.

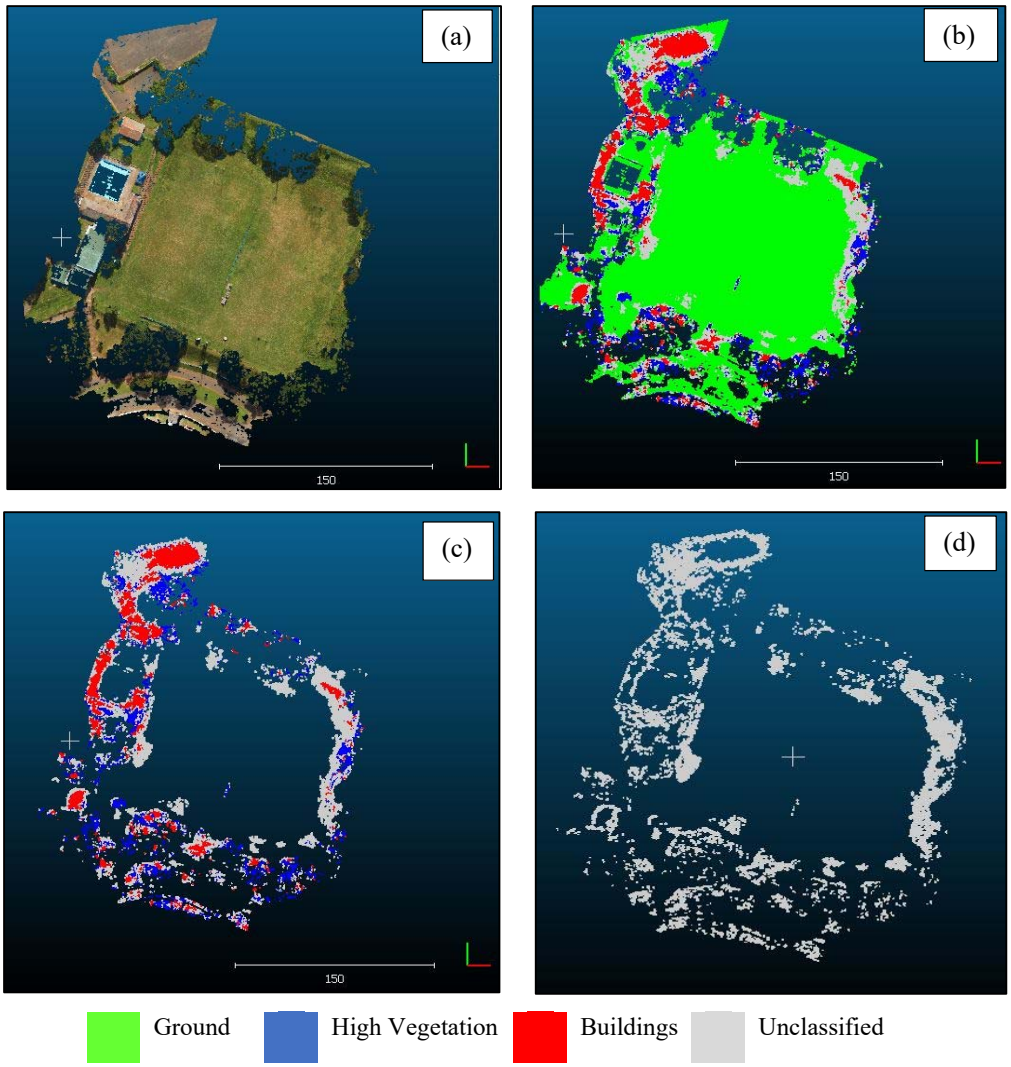

Figure 4: (a) Study area before classification; (b) Classified point cloud showing all classes; (c) Classified point cloud showing high vegetation and buildings (ground class removed); and (d) Unclassified points.

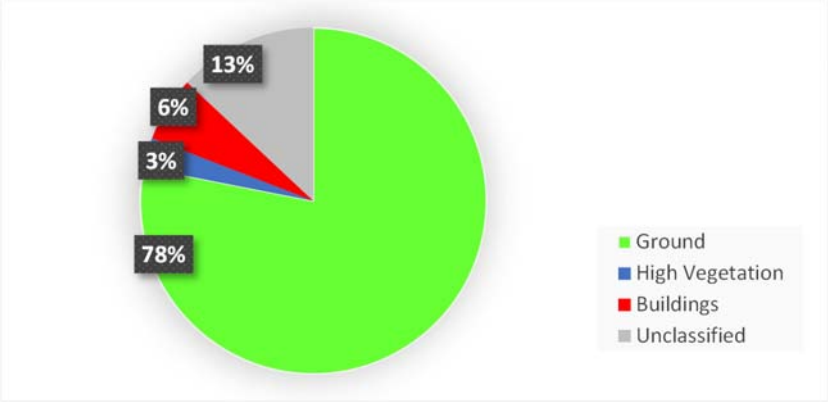

Figure 5: Percentage number of points classified in each land-cover category

About 13% of the points were not allocated to any class. In most cases, the unclassified points were located on sites where a possible intermediate land-cover category was observed. For example, the high vegetation and ground categories were found to be separable. Furthermore, the high grass on the site appeared to be unclassified, but in some cases, it was categorized as either ground or high vegetation. Another similar occurrence appeared where the steps were unclassified or classified as either ground or buildings. Both classification algorithms achieved results that were more-or-less similar.

Table 3 presents the results of the qualitative accuracy assessment. The ratings used in Table 3 are explained in Table 4.

Table 3: Qualitative assessment of classification algorithms

Feature	**Dominant Error**	**CANUPO rating**
Ground	Type II	***
High Vegetation	Type II	***
Buildings	Type I	**
		Pix4D Mapper rating
Ground	Type II	***
High Vegetation	Type I	***
Buildings	Type I	**

*: poor, **: fair, ***: good.

Table 4: Explanation of ratings

Rating	Item filter rating	Influence rating
Poor	Item not filtered most of the time (<50%)	Large influence on neighbouring points
Fair	Item not filtered a few times	Small influence on neighbouring points
Good	Item filtered most of the time (<90%)	None

The ground category achieved good results for both algorithms. In fact, this category was affected by only a few cases of the Type II error. Fair results were obtained in the building category. The Type I error was dominant in both filtering algorithms. Pix4D Mapper indicated more cases of the Type I error for the high vegetation category, while the CANUPO classification was associated with Type II errors.

The results of the quantitative accuracy assessment of the CANUPO classification are shown in the confusion matrix in Table 5. The reference and classified data indicate the number of ground truth sites and the classified sites, respectively.

Table 5: Confusion matrix of CANUPO classification

	Reference Data						
		Ground	**High Vegetation**	**Buildings**	**Sum**	**UA (%)**	**EC (%)**
Classified Data	**Ground**	36	2	1	39	92.3	7.69
	High Vegetation	2	18	2	22	81.8	18.18
	Buildings	2	1	11	14	78.6	21.43
	Unclassified	2	1	2	5		
	Sum	42	22	16	80		
	PA (%)	85.7	81.8	68.8			
	EO (%)	14.29	18.18	31.25			
	OA (%)	81.25					
	$\hat{k}$	0.70					

The performance of the CANUPO classification achieved an overall accuracy of 81.3%. The corresponding Kappa coefficient of 0.70 was achieved, indicating a substantial agreement according to the Kappa ratings. The ground category was less affected by errors of omission and commission. Misclassifications were noticed where sharp edges with slopes on the ground were classified as buildings. This was due to the geometry of points similar to those in the building category. The building category was mainly affected by both errors of omission (EO) and errors of commission (EC). It was noticed that flat rooftops were classified as either ground or unclassified. The training

samples used for the building category were mainly 3D by nature, while the ground category samples on most scales were 2D.

5. Discussion and Conclusion

The quality of 3D UAS-SfM point clouds produced in this study was affected mainly by discontinuities. In contrast to the LIDAR point clouds used by Brodu and Lague (2012), Farella (2016) Bonneau and Hutchinson (2019), the 3D photogrammetric point cloud used in this study was associated with some data discontinuities. This appeared to be a significant factor contributing to misclassifications. Another was the mixed pixel problem, which occurs when different classes on the observation scale contribute to the pixel's observed spectral response (Deer and Eklun, 2003). As a result, approximately 13% of the points did not belong to any class. Also, the buildings where side views were not reconstructed were classified as either ground or unallocated. The UAS images from which the point cloud was generated were vertical (nadir), lacking data from the side views. However, the incorporation of oblique images might address this issue during the SfM process since it improves the final point cloud by reducing data discontinuities and systematic errors (Nesbit and Hugenholtz, 2019). Initially, the water body (swimming pool) was one of the land-cover categories of interest. However, this category was eliminated because the 3D point cloud that was generated did not have the water body adequately reconstructed. The swimming pool category was associated with discontinuities.

A comparison with related studies on classifying 3D UAS-SfM point clouds was conducted. Zeybek and Şanlıoğlu (2019) classified ground and non-ground points by using different filtering algorithms. This work evaluated the performance of different filtering algorithms on UAS-based point clouds. Although these algorithms are mainly used to classify LIDAR data, the results indicated that UAS-SfM point cloud data are suitable for classifying bare earth surface features. Also, Zeybek (2021) classified 3D UAS-SfM point cloud data in the urban environment on the basis of their geometric properties. The overall classification accuracy was 96%, and the associated Kappa index was 91%. Similarly, the present study classified the 3D UAS-SfM point cloud data in the urban environment, achieving comparable accuracy. However, improving the classification accuracy and addressing the misclassifications are essential measures to take if reliable results are to be achieved.

The dimensionality of an object is the main component in a CANUPO classification. The results revealed that extracting classifiers from the point cloud subject to classification provides excellent results. However, in this study, the classifiers created were applied to a scene that had never been seen before. The CANUPO classification threshold also affected the classification results. It was noticed that a classification threshold of 100% provided fair results, with fewer points correctly classified for a particular class. The other class would then be the most likely to be affected by errors of commission. Classifier A separated ground from non-ground points; a classification threshold of 100% resulted in some ground points being classified as non-ground or unclassified. The threshold for Classifier A was reduced to 90% and produced improved results. The second classifier, Classifier

B, was initially applied at a threshold of 90%. Improved results were achieved at a threshold of 85%. It was noticed that by reducing the classification threshold, the results for both classifiers could be improved upon.

This study has demonstrated that photogrammetric products of good quality can be produced by using the low-cost UAS-SfM technique. Satisfactory CANUPO classification results were achieved, thus indicating the potential use of 3D UAS-SfM point clouds in mapping heterogeneous urban environments and other applications that might arise, and moreover, in advancing the recognition and use of free and open-source software for application in classification problems. Future research possibilities lie in the exploration of underwater environments and the possibility of combining terrestrial and aquatic point cloud data. Furthermore, yet another avenue for research would be to develop a 3D point cloud classification model that can classify objects of interest that are submerged underwater.

6. Acknowledgments

Acknowledgments are due to the South African National Research Foundation (NRF) for providing support. We also acknowledge the reviewers for their contributions in improving upon this paper.

7. References

Antonarakis, AS, Richards, KS & Brasington, J 2008. 'Object-based land cover classification using airborne LIDAR', *Remote Sensing of Environment*, vol. 112, no. 6, pp. 2988-2998.

Becker, C, Rosinskaya, E, Häni, N, d'Angelo, E & Strecha, C 2018, 'Classification of aerial photogrammetric 3D point clouds', *Photogrammetric Engineering & Remote Sensing*, vol. 84, no. 5, pp. 287-295.

Bonneau, DA & Hutchinson, DJ 2019, 'The use of terrestrial laser scanning for the characterization of a cliff-talus system in the Thompson River Valley, British Columbia, Canada', *Geomorphology*, vol. 327, pp. 598-609.

Boon, MA, Greenfield, R & Tesfamichael, S 2016, 'Unmanned aerial vehicle (UAV) photogrammetry produces accurate high-resolution orthophotos, point clouds and surface models for mapping wetlands', *South African Journal of Geomatics*, vol. 5, no. 2, pp. 186-200.

Brodu, N & Lague, D 2012, '3D terrestrial LIDAR data classification of complex natural scenes using a multi-scale dimensionality criterion: Applications in Geomorphology'. *ISPRS Journal of Photogrammetry and Remote Sensing*, vol. 68, pp. 121-134.

Calvo, JAL, Alirezaei, G & Mathar, R 2017, 'Wireless powering of drone-based MANETs for disaster zones', *2017 IEEE International Conference on Wireless for Space and Extreme Environments (WiSEE)*, Montreal, October 2017, pp. 98-103, IEEE, Canada, 2017.

Croce, V, Caroti, G, De Luca, L, Jacquot, K, Piemonte, A & Véron, P 2021, 'From the Semantic Point Cloud to Heritage-building Information Modeling: A Semi-automatic Approach exploiting Machine Learning', *Remote Sensing*, vol. 13, no. 3, p. 461.

Deer, PJ and Eklund, P 2003, 'A study of parameter values for a Mahalanobis distance fuzzy classifier', *Fuzzy Sets and Systems*, vol. 137, no. 2, pp.191-213.

DJI, 2017, DJI, Nanshan District, Shenzhen, viewed 20 January 2023, <https://www.dji.com/phantom>.

Farella, EM 2016, '3D Mapping of Underground Environments with a Hand-held Laser Scanner', Proceedings of the SIFET Congress, Lecce, pp. 48–57, SIFET, Italy, 2016.

Fetić, A, Jurić, D & Osmanković, D 2012, 'The procedure of a camera calibration using Camera Calibration Toolbox for MATLAB', *2012 Proceedings of the 35th International Convention MIPRO, Opatija, May 2012,* pp. 1752-1757, IEEE, Croatia, 2012.

Furukawa, Y, Curless, B, Seitz, SM & Szeliski, R 2010, 'Towards internet-scale multi-view stereo', *2010 IEEE Computer Society Conference on Computer Vision and Pattern Recognition,* San Francisco, June 2010, pp. 1434-1441, IEEE, California, 2010.

Furukawa, Y & Ponce, J 2009, 'Accurate, dense, and robust multiview stereopsis', *IEEE Transactions on Pattern Analysis and Machine Intelligence*, vol. 32, no. 8, pp.1362-1376.

Garcia, MVY & Oliveira, HC 2020, 'The influence of ground control point configuration and camera calibration for DTM and orthomosaic generation using imagery obtained from low-cost UAV. *ISPRS Annals of Photogrammetry, Remote Sensing and Spatial Information Sciences*', vol. *5, no.* 1, pp. 239-244.

Geavis, 2020, Why GCPs are Needed in Photogrammetry?, Geavis, Slovenia, viewed 20 August 2022, <https://www.geavis.si>

GEOIM, n.d., *Trimble R4 GNSS System*, GEOIM, Turkey, viewed 20 January 2023, <https://www.geoim.net/wp-content/uploads/2020/11/Trimble-Leica.pdf>.

Gevaert, CM., Persello, C & Vosselman, G 2016, 'Optimizing multiple kernel learning for the classification of UAV data', *Remote Sensing*, vol. 8, no. 12, p. 1025.

Grilli, E, Menna, F & Remondino, F 2017, 'A review of point cloud segmentation and classification algorithms', *The International Archives of Photogrammetry, Remote Sensing and Spatial Information Sciences*, vol. 42, pp.339-344.

Henrico, I, Combrinck, L & Eloff, C 2016, 'Accuracy comparison of Pléiades satellite ortho-images using GPS-device-based GCPs against TerraSAR-X-based GCPs', *South African Journal of Geomatics*, vol. 5, no. 3, pp. 358-372.

Hernandez-Lopez, D, Felipe-Garcia, B, Gonzalez-Aguilera, D & Arias-Perez, B 2013. 'An automatic approach to UAV flight planning and control for photogrammetric applications', *Photogrammetric Engineering & Remote Sensing*, vol. 79, no. 1, pp.87-98.

Jurado, JM, Cárdenas, JL, Ogayar, CJ, Ortega, L & Feito, FR 2020, 'Semantic Segmentation of Natural Materials on a Point Cloud using Spatial and Multispectral Features', *Sensors*, vol. 20, no. 8, p. 2244.

Lalonde, JF, Vandapel, N, Huber, DF & Hebert, M 2006, 'Natural terrain classification using three-dimensional ladar data for ground robot mobility', *Journal of Field Robotics*, vol. 23, no.10, pp. 839-861.

Liu, K & Boehm, J 2015, 'Classification of big point cloud data using cloud computing' *ISPRS-International Archives of the Photogrammetry, Remote Sensing and Spatial Information Sciences*, vol. 40, pp. 553-557.

Lucieer, A, Turner, D, King, D & Robinson, S 2013, 'Using an Unmanned Aerial Vehicle (UAV) to capture micro-topography of Antarctic moss beds', *International Journal of Applied Earth Observation and Geoinformation*, vol. 27, pp. 53-62.

Martínez-Carricondo, P, Agüera-Vega, F, Carvajal-Ramírez, F, Mesas-Carrascosa, FJ, García-Ferrer, A & Pérez-Porras, FJ 2018, 'Assessment of UAV-photogrammetric mapping accuracy based on variation of ground control points', International *Journal of Applied Earth Observation and Geoinformation*, vol. 72, pp. 1-10.

Nedevschi, S, Marita, T, Vaida, M, Danescu, R, Frentiu, D, Oniga, F, Pocol, C & Moga, D 2002, 'Camera Calibration Method for Stereo Measurements', *Journal of Control Engineering and Applied Informatics (CEAI)*, vol. *4*, no. 2, pp.21-28.

Nesbit, PR, & Hugenholtz, CH 2019, 'Enhancing UAV–SFM 3D model accuracy in high-relief landscapes by incorporating oblique images', *Remote Sensing*, vol. 11, no. 3, p.239.

Niemeyer, J, Rottensteiner, F & Soergel, U 2012, 'Conditional random fields for LIDAR point cloud classification in complex urban areas', *ISPRS Annals of Photogrammetry, Remote Sensing and Spatial Information Sciences*, vol. 1, no. 3, pp .263-268.

Ouédraogo, M, Degré, A, Debouche, C & Lisein, J 2014, 'The evaluation of unmanned aerial system-based photogrammetry and terrestrial laser scanning to generate DEMs of agricultural watersheds', *Geomorphology*, vol. 214, pp. 229-355.

Pix4D, 2021, Pix4D, Switzerland, viewed 23 June 2021, <https://www.pix4d.com>.

Pix4DSA, 2019, Pix4D, Switzerland, viewed 13 July 2020, <https://www.pix4d.com>.

Roynard, X, Deschaud, JE & Goulette, F 2018, 'Classification of point cloud scenes with multi-scale voxel deep network', *arXiv preprint arXiv:1804.03583*.

Sithole, G & Vosselman, G 2004, 'Experimental comparison of filter algorithms for bare-Earth extraction from airborne laser scanning point cloud', *ISPRS Journal of Photogrammetry and Remote Sensing*, vol 59, no. 1-2, pp.85-101.

Snavely, N, Seitz, SM & Szeliski R 2008, 'Modeling the world from internet photo collections', *International Journal of Computer Vision*, vol. 80, no. 2, pp. 189-210.

Theodoridis, S & Koutroumbas, K 2008, *Pattern Recognition*, 4th edition, Academic Press Inc., United States of America.

Tiscareño, J, Albajez, JA & Santolaria, J 2019, 'Analysis of different camera calibration methods on a camera-projector measuring system', *Procedia Manufacturing*, vol. 41, pp. 539-546.

UKZN – University of KwaZulu-Natal 2017, University of KwaZulu-Natal, Glenwood, Durban, South Africa, viewed 13 July 2021, <https://ukzn.ac.za/about-ukzn/campuses/>.

Van Genechten, B 2008, *Theory and practice of Terrestrial Laser Scanning: Training material based on practical applications*, Universidad Politecnica de Valencia Editorial, Valencia, Spain.

Vandapel, N, Huber, DF, Kapuria, A & Hebert, M 2004, 'Natural terrain classification using 3D ladar data', In: *IEEE International Conference on Robotics and Automation, 2004. Proceedings. ICRA'04. 2004*, New Orleans, April 2004, pp. 5117-5122, IEEE, USA, 2004.

Wallace, L, Lucieer, A, Watson, C & Turner, D 2012, 'Development of a UAV-LIDAR system with application to forest inventory', *Remote Sensing*, vol. 4, no. 6, pp. 1519-1543.

WebODM – OpenDroneMap, 2021 GitHub Inc, San Francisco, California, United States, viewed 20 June 2021, <https://github.com/OpenDroneMap/WebODM>.

Weinmann, M, Jutzi, B, Hinz, S & Mallet, C 2015, 'Semantic point cloud interpretation based on optimal neighborhoods, relevant features and efficient classifiers', *ISPRS Journal of Photogrammetry and Remote Sensing*, vol. 105, pp. 286-304.

Westoby, MJ, Brasington, J, Glasser, NF, Hambrey, MJ & Reynolds, JM 2012, 'Structure-from-Motion'photogrammetry: A low-cost, effective tool for geoscience applications', *Geomorphology*, vol. 179, pp. 300-314.

Wheeler, M, Schrick, B, Whitacre, W, Campbell, M, Rysdyk, R & Wise, R 2006, 'Cooperative tracking of moving targets by a team of autonomous UAVs, *2006 IEEE/AIAA 25th Digital Avionics Systems Conference,* 2006. IEEE, pp. 1-9.

Yusoff, AR, Ariff, MM, Idris, KM, Majid, Z & Chong, AK 2017. 'Camera calibration accuracy at different UAV flying heights', *The International Archives of Photogrammetry, Remote Sensing and Spatial Information Sciences*, vol. 42, pp. 595-600.

Zeybek, M, 2021, 'Classification of UAV point clouds by random forest machine learning algorithm', *Turkish Journal of Engineering*, vol. 5, no. 2, pp. 48-57.

Zeybek, Ma & Şanlıoğlu, İ 2019, 'Point cloud filtering on UAV-based point cloud', *Measurement*, vol. 133, pp. 99-111.

Zhang, C & Kovacs, JM 2012, 'The application of small unmanned aerial systems for precision agriculture: a review', *Precision Agriculture*, vol. 13, no. 6, pp. 693-712.

Zhang, Z 2000, 'A flexible new technique for camera calibration', *IEEE Transactions on Pattern Analysis and Machine Intelligence*, vol. 22, no. 11, pp. 1330-1334.